Numerical Study of Vortex Interactions in Bose-Einstein Condensation

Yanzhi Zhang*

Department of Scientific Computing, Florida State University, Tallahassee, FL 32306-4120, USA

Abstract. The dynamics and interaction of quantized vortices in Bose-Einstein condensates (BECs) are investigated by using the two-dimensional Gross-Pitaevskii equation (GPE) with/without an angular momentum rotation term. If all vortices have the same winding number, they would rotate around the trap center but never collide. In contrast, if the winding numbers are different, their interaction highly depends on the initial distance between vortex centers. The analytical results are presented to describe the dynamics of the vortex centers when $\beta=0$. While if $\beta\neq 0$, there is no analytical result but some conclusive numerical findings are provided for the further understanding of vortex interaction in BECs. Finally, the dynamic laws describing the relation of vortex interaction in nonrotating and rotating BECs are presented.

PACS (2006): 03.75.Kk, 03.75.Lm, 05.30.Jp, 32.80.Pj

Key words: rotating Bose-Einstein condensation, Gross-Pitaevskii equation, angular momentum rotation, vortex interaction, vortex pair, vortex dipole.

1 Introduction

The first observation of a single vortex line in weakly interacting alkali gases has verified the superfluid properties of Bose-Einstein condensates (BECs) [1]. Recently, many efforts have been made to develop more complicated vortices. For example, vortex lattices containing a large number of vortices were created by rotating the system with a laser spoon [2, 3]; multiply charged vortices were also observed by using the topological phase engineering methods [4]. It is expected that more complicated vortex clusters can be created in the future with the further development of phase imprinting method. The achievement of vortex states would enable various opportunities, ranging from investigating the properties of random polynomials [5] to using vortices in quantum memories [6]. All of these developments have stirred interests in the study of states with several vortices.

*Corresponding author. *Email address:* yzhang5@fsu.edu (Y. Zhang)

So far, there have been a number of investigations on the properties of vortices in BECs. For example, the manipulation of the topological charge of a vortex by external potentials was discussed in [7]; different stationary vortex cluster states were observed in nonrotating BECs [8–10], and later the dynamical stability of these cluster was investigated in [11]. The interaction of vortices in nonrotating BECs was studied in [12] when the atomic interaction is very weak. The generation and dynamics of vortex-antivortex pairs were studied in a toroidal condensate [13]. By using the Thomas-Fermi approximation, analytical expressions for the angular momentum and the energy of a vortex dipole were obtained in [14].

The main aims of this paper are: i) to provide a detailed study of the vortex interaction in nonrotating BECs; ii) to extend the interaction study from nonrotating BECs to rotating condensates. There are four possible reasons affecting the vortex interaction: the winding number of a vortex, the initial distance between vortex centers, the strength of atomic interaction, and the angular rotation speed if in rotating BECs. To get an insight about the vortex interaction, we start by considering the interaction with zero atomic interaction, and find the analytical results to describe the motion of vortex centers. This study is extended by taking a small atomic interaction into account, and due to the nonlinear effect the dynamics become more complicated. To the best of our knowledge, there is still no study about the interaction of vortices in strongly interacting BECs. In this paper, we obtain some conclusive findings for the strongly interacting case, which may provide the further understanding of the vortex interaction in BECs. Finally, the vortex interaction in rotating BECs is studied. Analytical results are derived to show the relation between the interaction in nonrotating and rotating BECs. Some numerical results are also presented to verify our analytical findings.

The paper is organized as follows. In Section 2, the mathematical model and numerical schemes are introduced. In Section 3, the dynamics and interaction of one, two and more vortices are investigated in detail for nonrotating BECs. It is generalized to the rotating BECs in Section 4, and also a relation connecting the dynamics of vortices in nonrotating and rotating BECs is presented in Section 4. Section 5 provides a summary and brief discussion.

2 The mathematical model and numerical schemes

2.1 The mathematical model

At a temperature T much smaller than the critical temperature T_c, the properties of BECs in a rotational frame can be well described by the macroscopic wave function $\psi(\mathbf{x},t)$, whose evolution is governed by a self-consistent, mean field nonlinear Schrödinger equation (NLSE), also known as the Gross-Pitaevskii equation (GPE) with an angular momen-

tum rotation term [15,16]

$$i\hbar\partial_t\psi(\mathbf{x},t)=\left(-\frac{\hbar^2}{2m}\nabla^2+V(\mathbf{x})+NU_0|\psi|^2-\Omega L_z\right)\psi(\mathbf{x},t),\qquad \mathbf{x}\in\mathbb{R}^3,\quad t\geq 0,\tag{2.1}$$

where $\mathbf{x}=(x,y,z)\in\mathbb{R}^3$ is the Cartesian coordinate vector, m is the atomic mass, $\hbar$ is the Planck constant, N is the total number of atoms in the condensate, Ω is the angular velocity of the rotating laser beam and $U_0=4\pi\hbar^2a_s/m$ describes the interaction between atoms in the condensate with a_s (positive for repulsive interaction and negative for attractive interaction) the scattering length. $L_z=-i\hbar(x\partial_y-y\partial_x)$ is the z-component of the angular momentum $\mathbf{L}=\mathbf{x}\times(-i\hbar\nabla)$. The external potential is described by $V(\mathbf{x})$, and if a radially symmetric harmonic potential is considered, it takes the form

$$V(\mathbf{x})=\frac{m}{2}\left[\omega_r^2\left(x^2+y^2\right)+\omega_z^2z^2\right],\tag{2.2}$$

with ω_r and ω_z the trapping frequencies in the radial and axial directions, respectively. The wave function in (2.1) is normalized by

$$\|\psi(\cdot,t)\|^2:=\int_{\mathbb{R}^3}|\psi(\mathbf{x},t)|^2d\mathbf{x}=1,\qquad t\geq 0.\tag{2.3}$$

Under the normalization (2.3), we can introduce the dimensionless variables: $t\to t/\omega_r$, $\mathbf{x}\to a_0\mathbf{x}$ with $a_0=\sqrt{\hbar/m\omega_r}$, $\psi\to\psi/a_0^{3/2}$ and $\Omega\to\omega_r\Omega$, and obtain a dimensionless GPE [17–19]. If the condensate is tightly confined in the axial direction, i.e., $\omega_z\gg\omega_r$, the three-dimensional (3D) GPE can be further reduced to a two-dimensional (2D) GPE [17–19]. In this paper, we will use the following 2D dimensionless GPE as our study model:

$$i\frac{\partial\psi(\mathbf{x},t)}{\partial t}=\left[-\frac{1}{2}\left(\frac{\partial^2}{\partial x^2}+\frac{\partial^2}{\partial y^2}\right)+\frac{1}{2}(x^2+y^2)+\beta|\psi|^2-\Omega L_z\right]\psi(\mathbf{x},t),\qquad t\geq 0,\tag{2.4}$$

$$\psi(\mathbf{x},0)=\psi_0(\mathbf{x})\quad\text{with}\quad\|\psi_0\|^2:=\int_{\mathbb{R}^2}|\psi_0(\mathbf{x})|^2d\mathbf{x}=1,\tag{2.5}$$

where $\mathbf{x}=(x,y)\in\mathbb{R}^2$, $L_z=-i(x\partial_y-y\partial_x)$ and β is a constant characterizing the strength of the interatomic interaction. There are two important invariants of the GPE (2.4)-(2.5): the normalization of the wave function

$$\|\psi(\cdot,t)\|^2=\int_{\mathbb{R}^2}|\psi(\mathbf{x},t)|^2d\mathbf{x}\equiv\int_{\mathbb{R}^2}|\psi(\mathbf{x},0)|^2d\mathbf{x}=1,\quad t\geq 0,\tag{2.6}$$

and the energy

$$E(\psi)=\int_{\mathbb{R}^2}\left[\frac{1}{2}|\nabla\psi|^2+\frac{1}{2}(x^2+y^2)|\psi|^2+\frac{\beta}{2}|\psi|^4-\Omega\mathrm{Re}(\psi^*L_z\psi)\right]d\mathbf{x}\equiv E(\psi_0),\quad t\geq 0,\tag{2.7}$$

where f^* and $\mathrm{Re}(f)$ denote the conjugate and real part of the function f, respectively.

To find the stationary vortex state, we can rewrite the wave function $\psi(\mathbf{x},t)$ into the form [17,19–21]

$$\psi(\mathbf{x},t)=\phi_m(\mathbf{x})e^{-i\mu_m t}=f_m(r)e^{im\theta}e^{-i\mu_m t}, \tag{2.8}$$

where (r,θ) is the polar coordinate, $m\in\mathbb{Z}$ is the winding number (or topological charge) of the vortex, and μ_m is the chemical potential defined by

$$\mu_m=\int_{\mathbb{R}^2}\left[\frac{1}{2}|\nabla\phi_m|^2+\frac{1}{2}(x^2+y^2)|\phi_m|^2+\beta|\phi_m|^4-\Omega\mathrm{Re}(\phi_m^* L_z\phi_m)\right]d\mathbf{x}. \tag{2.9}$$

The real-valued modulus $f_m(r)$ satisfies

$$\mu_m f_m(r)=\left[-\frac{1}{2r}\frac{d}{dr}\left(r\frac{d}{dr}\right)+\frac{1}{2}\left(r^2+\frac{m^2}{r^2}\right)+\beta|f_m(r)|^2+m\Omega\right]f_m(r), \tag{2.10}$$

$$f_m(0)=0,\quad \lim_{r\to\infty}f_m(r)=0\quad\text{with}\quad 2\pi\int_0^\infty|f_m(r)|^2 r\,dr=1. \tag{2.11}$$

In the case of $\beta=0$, Eqs. (2.10)-(2.11) can be exactly solved and [17,19]

$$f_{m,\beta=0}(r)=\frac{1}{\sqrt{\pi|m|!}}r^{|m|}\exp\left(-\frac{r^2}{2}\right),\qquad r\geq 0. \tag{2.12}$$

While when $\beta\neq 0$, there is no exact solution to $f_m(r)$, but it can be obtained by solving (2.10)-(2.11) numerically. In this paper, we will study the dynamics and interaction of n vortices with winding number $m=\pm 1$. To do this, we set the initial condition in (2.5) as

$$\psi_0(\mathbf{x})=\alpha\prod_{j=1}^n\phi_{m_j}(\mathbf{x}-\mathbf{x}_j^0)=\alpha\prod_{j=1}^n\phi_{m_j}(x-x_j^0,y-y_j^0),\qquad \mathbf{x}\in\mathbb{R}^2, \tag{2.13}$$

where $\mathbf{x}_j^0=(x_j^0,y_j^0)$ and $m_j=\pm 1$ define the initial position and the winding number of the j-th vortex for $j=1,2,\ldots,n$, respectively; the constant α is chosen such that the initial data (2.13) satisfies the normalization condition in (2.5).

2.2 Numerical schemes

There are numerous available numerical methods to solve the time-dependent GPE (2.4)-(2.5). For example, a set of finite difference schemes was presented and applied in [22–24]; recently the quantum lattice Boltzmann (qLB) schemes were proposed to study the steady states and dynamics of nonrotating BECs [25,26]. In this paper, we will apply the time-splitting spectral type methods in [17,18,27] to solve the GPE (2.4) with/without a rotation term. The main merit of these methods is that they are of high-order accuracy and unconditionally stable. For the convenience of the reader, in the following we give a brief review of these methods.

To solve the GPE (2.4)-(2.5), we first truncate the problem into a bounded computational domain with the homogeneous Dirichlet boundary condition, i.e.,

$$i\partial_t\psi(\mathbf{x},t) = -\frac{1}{2}(\partial_x^2+\partial_y^2)\psi+\frac{1}{2}(x^2+y^2)\psi+\beta|\psi|^2\psi-\Omega L_z\psi, \quad \mathbf{x}\in\Omega_{\mathbf{x}}, \quad t>0, \tag{2.14}$$

$$\psi(\mathbf{x},t)=0, \quad \mathbf{x}\in\Gamma=\partial\Omega_{\mathbf{x}}, \quad t\geq 0, \tag{2.15}$$

$$\psi(\mathbf{x},0)=\psi_0(\mathbf{x}), \quad \mathbf{x}\in\overline{\Omega}_{\mathbf{x}}, \tag{2.16}$$

where the computational domain is defined by $\Omega_{\mathbf{x}}=[a,b]\times[c,d]$. Due to the confinement of the external potential, the solution of (2.4)-(2.5) decays exponentially fast to zero when $|\mathbf{x}|\to\infty$; thus if we choose $|a|,b,|c|$ and d sufficiently large, the effect of the domain truncation can be neglected.

Choose a time step size $\Delta t>0$ and define the time sequence $t_n=n\Delta t$ for $n=0,1,\ldots$. Then from time $t=t_n$ to $t=t_{n+1}$, the GPE (2.14) can be solved in the following two steps:

$$i\partial_t\psi(\mathbf{x},t) = -\frac{1}{2}(\partial_x^2+\partial_y^2)\psi+i\Omega(x\partial_y-y\partial_x)\psi, \tag{2.17}$$

$$i\partial_t\psi(\mathbf{x},t) = \frac{1}{2}(x^2+y^2)\psi+\beta|\psi|^2\psi. \tag{2.18}$$

Eq. (2.18) can be integrated exactly in time, and we have

$$\psi(\mathbf{x},t)=\psi(\mathbf{x},t_n)\exp\left[-i\left(\beta|\psi(\mathbf{x},t_n)|^2+(x^2+y^2)/2\right)(t-t_n)\right] \quad \text{for} \quad t\in[t_n,t_{n+1}]. \tag{2.19}$$

For Eq. (2.17), we use different discretizations when $\Omega=0$ and $\Omega\neq 0$.

When $\Omega=0$, we choose the spatial mesh size $\Delta x=(b-a)/J$ and $\Delta y=(d-c)/K$ with J, K two even positive integers, and denote the grid points $x_j=a+j\Delta x$ (for $j=0,1,\ldots,J$) and $y_k=c+k\Delta y$ (for $k=0,1,\ldots,K$). Let $\psi_{j,k}^n$ be the approximation of $\psi(x_j,y_k,t_n)$. Then Eq. (2.17) can be discretized by the sine pseudospectral method in space and integrated exactly in time, i.e. we have

$$\psi_{j,k}(t)=\sum_{p=1}^{J-1}\sum_{q=1}^{K-1}\left(\widehat{\psi_{p,q}^n}\exp(-i(\mu_p^2+\lambda_q^2)(t-t_n)/2)\right)\sin(\mu_p(x_j-a))\sin(\lambda_q(y_k-c), \tag{2.20}$$

for $t\in[t_n,t_{n+1}]$, where $\widehat{\psi_{p,q}}$ are the sine-transform coefficients defined by

$$\widehat{\psi_{p,q}}=\frac{4}{JK}\sum_{j=1}^{J-1}\sum_{k=1}^{K-1}\psi_{j,k}\sin(\mu_p(x_j-a))\sin(\lambda_q(y_k-c)) \quad \text{with} \quad \mu_p=\frac{p\pi}{b-a}, \quad \lambda_q=\frac{q\pi}{d-c}.$$

Then the full scheme for the GPE (2.14)-(2.16) can be obtained by combining (2.19) and (2.20) through the fourth-order splitting-step method, i.e., the fourth-order time-splitting sine pseudospectral (TSSP4) method; see [17] for more details. This method is of spectral accuracy in space and the fourth-order accuracy in time. It is unconditionally stable,

time reversible and time transverse invariant. It also conserves the normalization in the discrete level [17].

While when $\Omega \neq 0$, the nonlinear coefficient of the angular momentum rotation term makes the sine pseudospectral discretization not work for (2.17), so that the above TSSP4 method can not be used to solve the GPE (2.14) in a rotating frame. However, we can formulate (2.17) into the polar coordinate and have

$$i\partial_t \psi(\mathbf{x},t) = -\frac{1}{2r}\frac{\partial}{\partial r}\left(r\frac{\partial \psi}{\partial r}\right) - \frac{1}{2r^2}\frac{\partial^2 \psi}{\partial \theta^2} + i\Omega\frac{\partial \psi}{\partial \theta}. \tag{2.21}$$

Eq. (2.21) can be discretized in the θ-direction by a Fourier pseudospectral method, in the r-direction by a fourth or sixth-order finite difference method, and in time by a Crank-Nicolson method. Then the steps (2.17) and (2.18) are coupled by the second-order time-splitting method. The resulting scheme is also unconditionally stable and time reversible (see the detailed scheme in [18]). It will be used in Section 4 to study the dynamics and interaction of vortices in rotating BECs.

In addition, a leap-frog Fourier pseudospectral (LFFP) method was proposed in [27]. The LFFP method applying the Cartesian coordinate is explicit and of spectral accuracy in all direction. However, it is conditionally stable.

3 Vortices in nonrotating BECs

In this section, we investigate the dynamics and interaction of vortices in nonrotating BECs. The GPE (2.14)-(2.16) with $\Omega = 0$ is solved by using the fourth-order time-splitting sine spectral (TSSP4) method.

For a special case, if we choose $n = 1$ in (2.13), i.e. there is only one vortex, the motion of its center can be described by the second-order ODE system [18, 27–29]:

$$x''(t) + x(t) = 0, \quad y''(t) + y(t) = 0, \qquad t \geq 0, \tag{3.1}$$

$$x(0) = x^0, \quad y(0) = y^0, \quad x'(0) = y'(0) = 0, \tag{3.2}$$

where $\mathbf{x}(t)$ and $\mathbf{x}^0$ denote the locations of the vortex center at time $t > 0$ and $t = 0$, respectively. From (3.1)-(3.2), it is easy to obtain

$$x(t) = x^0 \cos t, \quad y(t) = y^0 \cos t, \qquad t \geq 0. \tag{3.3}$$

That is, the vortex moves on a straight line, and its dynamics depends only on the initial position (x^0, y^0), but not on the nonlinear parameter β or the winding number m.

In contrast to the single vortex, the dynamics of $n \geq 2$ vortices are much more complicated. In the following, we will start from considering the interaction of two vortices with the same or opposite winding numbers, and then generalize it to the case with more vortices, i.e. for $n \geq 3$ in (2.13).

3.1 Interaction of vortex pair

A vortex pair is defined as two vortices having the same winding number, i.e. $n=2$, and

$$m_1=m_2=m, \quad \text{with} \quad m=+1 \text{ or } -1 \tag{3.4}$$

in the initial condition (2.13). To get an insight into the interaction of a vortex pair and as a background against the results found for the weakly and strongly interacting condensate, we first consider the interaction when $\beta=0$. Since the support region of a single vortex is small when $\beta=0$, to apply the initial setup in (2.13), the initial distance between two centers can not be too large.

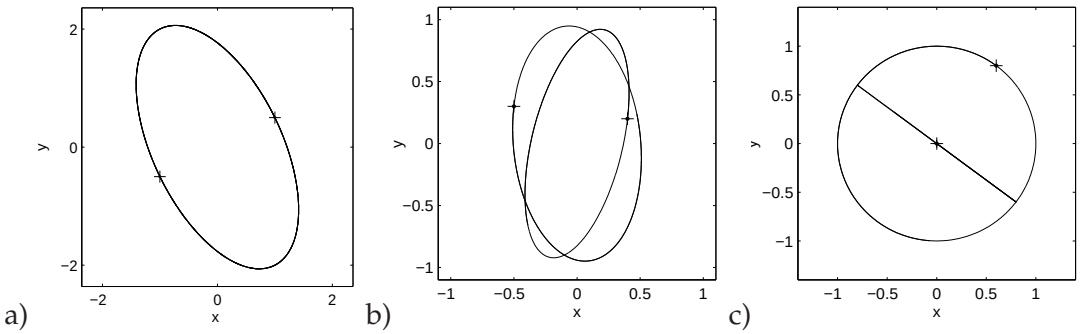

Figure 1: Trajectory of vortex pairs when $\beta=0$ and $m=1$. a) $\mathbf{x}_{1,2}^0=(\pm1,\pm0.5)$; b). $\mathbf{x}_1^0=(-0.5,0.3)$ and $\mathbf{x}_2^0=(0.4,0.2)$; c). $\mathbf{x}_1^0=(0.6,0.8)$ and $\mathbf{x}_2^0=(0,0)$.

Figure 1 shows the trajectory of a vortex pair with different initial positions. We can rewrite the wave function into the form

$$\psi(\mathbf{x},t)=\sqrt{\rho(\mathbf{x},t)}\exp\left(iS(\mathbf{x},t)\right), \qquad \mathbf{x}\in\mathbb{R}^2, \quad t\geq 0, \tag{3.5}$$

and define $\rho(\mathbf{x},t)=|\psi|^2$ and $S(\mathbf{x},t)=\arg(\psi)$ as the position density and the phase of the wave function, respectively. Figure 2 displays the time evolution of the phase $S(\mathbf{x},t)$ and the density $|\psi(\mathbf{x},t)|$ for the case with $\mathbf{x}_{1,2}^0=(\pm1,\pm0.5)$ and $m_1=m_2=1$. In all trajectory figures, we use '$+$' and '$\times$' to represent the initial position of the vortices which have the winding number $+1$ and -1, respectively. While in the plots of the phase and position density, these symbols represent the position of the vortex centers at a specified time.

From Figs. 1-2, we find that the two vortices having the same winding number never collide with each other. During the dynamics, they would rotate (clockwise when $m=-1$ and counter clockwise when $m=+1$) around the trap center with period $T=2\pi$. Furthermore, if initially the two vortices are symmetrically located with respect to the trap center, then their trajectories are exactly the same and $\mathbf{x}_1(t)=-\mathbf{x}_2(t)$ for any time $t\geq 0$ (c.f. Fig. 1a). In addition, our additional simulations show that during the dynamics there are always two vortices in the condensate.

In fact, when $\beta=0$, we have the following lemma for the dynamics of a vortex pair in nonrotating BECs:

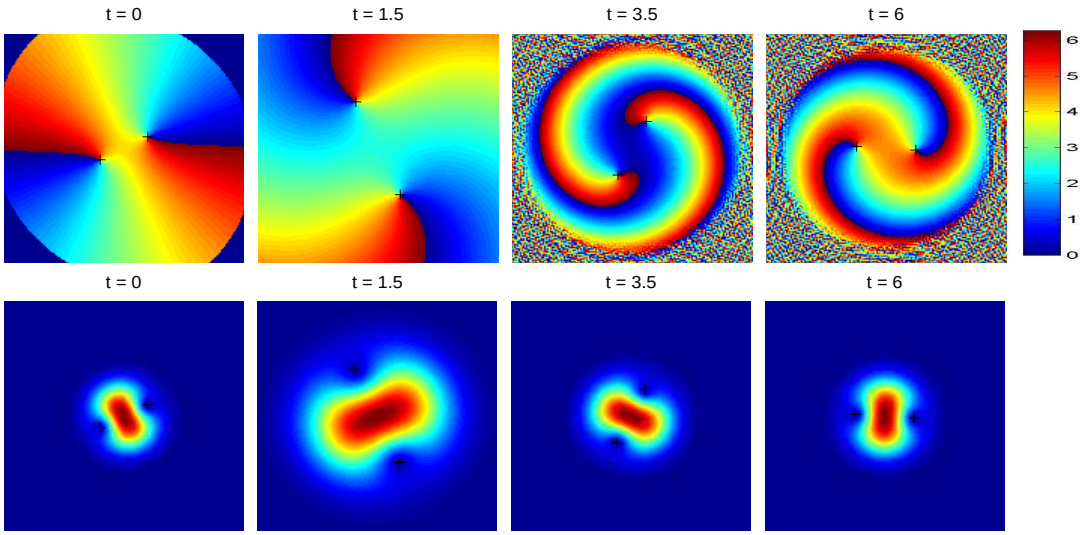

Figure 2: Plots of the phase $S(\mathbf{x},t)$ (above) and the density $|\psi(\mathbf{x},t)|$ (down) for a vortex pair with $\mathbf{x}_{1,2}^0 = (\pm 1, \pm 0.5)$ and $\beta = 0$, where the displayed domain is $[-5,5]\times[-5,5]$.

Lemma 3.1. *When $\beta = 0$ and $\Omega = 0$ in (2.4), if the initial data $\psi_0(\mathbf{x})$ is chosen as (2.13) with $n = 2$ and $m_1 = m_2 = m$, then the dynamics of the vortex centers can be described by the following second-order ODE system:*

$$x_j''(t) + x_j(t) = 0, \quad y_j''(t) + y_j(t) = 0, \qquad t \geq 0, \tag{3.6}$$

$$x_j(0) = x_j^0, \quad y_j(0) = y_j^0, \quad x_j'(0) = m(y_k^0 - y_j^0), \quad y_j'(0) = m(x_j^0 - x_k^0), \tag{3.7}$$

where $\mathbf{x}_j(t)$ represents the center of the j-th vortex at the time $t \geq 0$, and $j,k = 1,2$ but $k \neq j$.

Different from the dynamics of a single vortex described in (3.1)-(3.2), at time $t = 0$ the vortex pair has a nonzero velocity which depends on the relative location of their centers and their winding numbers.

The situation gets more complicated when a finite interaction parameter β is taken into account. To the best of our knowledge, there is still no literature addressing the interaction of vortices in strongly interacting BECs, i.e. when $\beta \gg 1$. Next we will start by considering the interaction in weakly interacting BECs to get an insight about the nonlinear effect on the interaction. To make the discussion easier, we assume that initially the two vortices are located at $\mathbf{x}_1^0 = (x_0, 0)$ and $\mathbf{x}_2^0 = (-x_0, 0)$ for $x_0 > 0$, and that their winding number are $m_1 = m_2 = m = +1$.

Figure 3 displays the trajectory of the vortex pairs in weakly (e.g. $\beta = 1$) and strongly (e.g. $\beta = 1000$) interacting BECs. Similar to the case of $\beta = 0$, if initially the two vortices are symmetric with respect to the trap center, then for any time $t \geq 0$ we have $\mathbf{x}_1(t) = -\mathbf{x}_2(t)$. Thus for simplicity, Fig. 3 only depicts the trajectory for $\mathbf{x}_1(t)$ with $\mathbf{x}_1^0 = (1,0)$. It shows that when $\beta \neq 0$, the dynamics and interaction of a vortex pair is no longer periodic. For

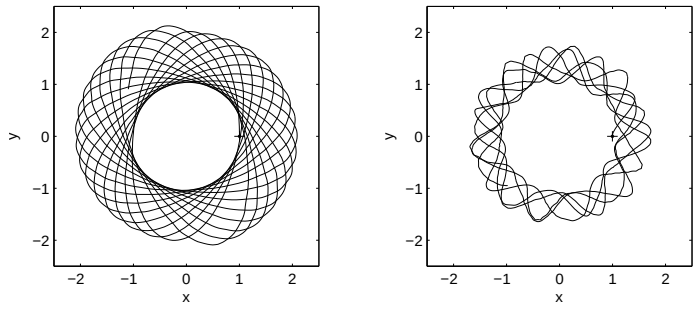

Figure 3: Trajectory of the vortex center $\mathbf{x}_1(t)$ for time $t\in[0,100]$, where $\mathbf{x}_1^0=(1,0)$, and $\beta=1$ (left) and $\beta=1000$ (right).

any time $t\geq 0$, the distance between two vortex centers is always larger than their initial distance $d_0=2x_0$. In contrast to the case of $\beta=0$, the two vortices have different trajectories even though their initial locations satisfy $\mathbf{x}_1^0=-\mathbf{x}_2^0$. However, their trajectories have the same envelopes which are two homocentric circles with radii $r_1=x_0<r_2(x_0,\beta)$, where the radius $r_2(x_0,\beta)$ depends on both x_0 and β.

In addition, our numerical results show that when $\beta\neq 0$, during the dynamics there may be additional vortices generated in the condensate. To understand the presence of these additional vortices, we denote $N_v(t)$ as the number of vortices appearing in the condensate at time t, and define

$$\langle N_v\rangle=\frac{1}{T}\int_0^T N_v(t)\,dt,\qquad T>0 \tag{3.8}$$

as the average number of vortices present during the time interval $[0,T]$. Figure 4 displays the average number $\langle N_v\rangle$ in the time interval $[0,25]$ for different β. It also shows the time evolution of $N_v(t)$ for $\beta=15$ and $x_0=1$. In addition, Figure 5 plots the time evolution of the phase $S(\mathbf{x},t)$ and the density $|\psi(\mathbf{x},t)|$ for $\beta=15$, and Figure 6 shows the density plots for $\beta=500$.

We see that for any time $t\geq 0$, there are always two vortices in the condensate, i.e. $\langle N_v\rangle\equiv 2$, if the interatomic interaction parameter β is too small or too large. Otherwise, the average number $\langle N_v\rangle>2$ and it reaches the maximum value at $\beta\approx 30$. The time evolution of $N_v(t)$ for $\beta=15$ shows that after some time (e.g. $t>9$), there are two additional vortices appearing in the condensate and they keep coming and going during the dynamics. Furthermore, Fig. 5 illustrates that the two additional vortices are always generated from the boundary of the condensate, and both of them have the same winding number as that of the vortex pair, i.e., $m=+1$. On the other hand, the results in Fig. 6 again confirm that for large β, there are always two vortices during the dynamics.

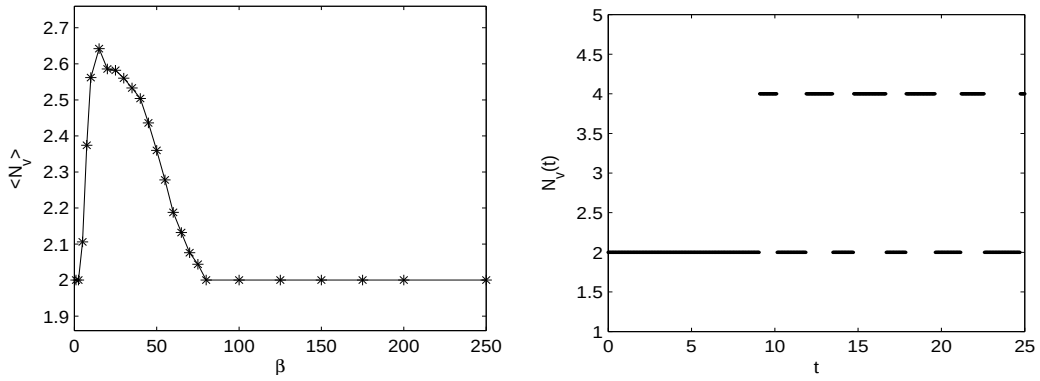

Figure 4: Average number of vortices $\langle N_v \rangle$ present in time interval $[0,25]$ (left) and the time evolution of $N_v(t)$ for $\beta=15$ (right), where $x_0=1$.

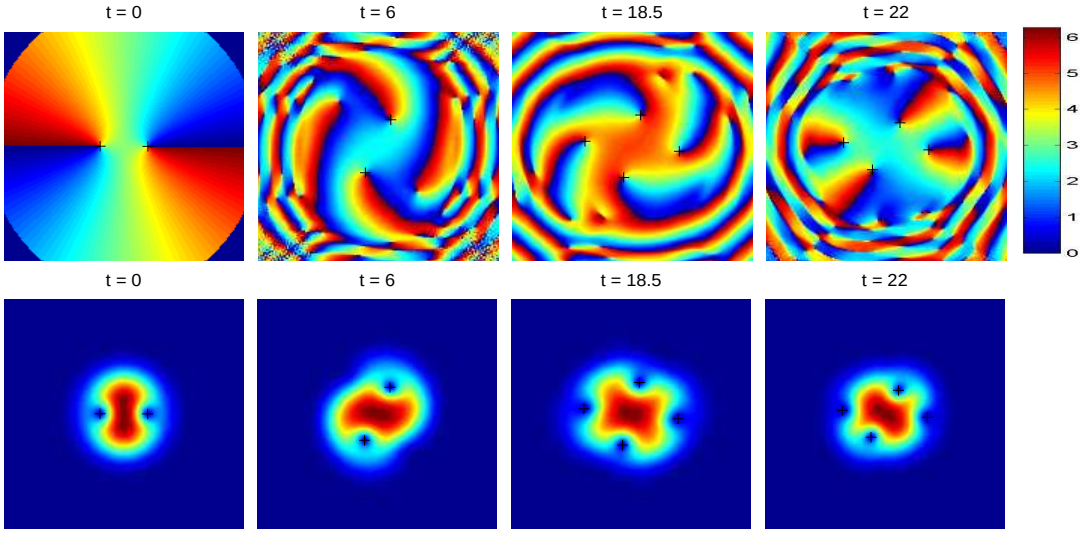

Figure 5: Plots of the phase $S(\mathbf{x},t)$ (above) and the density $|\psi(\mathbf{x},t)|$ (down) for a vortex pair with $\mathbf{x}_{1,2}^0=(\pm 1,0)$ and $\beta=15$, where the displayed domain is $[-5,5]\times[-5,5]$.

3.2 Interaction of vortex dipole

A vortex dipole consists of two vortices which have the opposite winding number, i.e.,

$$m_1=-m_2=m, \quad \text{with} \quad m=+1 \text{ or } -1. \tag{3.9}$$

Compared to the vortex pair, the dynamics and interaction of a vortex dipole highly depend on their initial distance $|\mathbf{x}_1^0-\mathbf{x}_2^0|$. Similarly, for the convenience of discussion, we assume that at $t=0$, the two vortices are located symmetrically with respect to the potential center $(0,0)$. Without loss of generality, we assume that the positive vortex, i.e., the vortex with $m=+1$, is initially located at $\mathbf{x}_1^0=(x_0,0)$, and the negative one with $m=-1$,

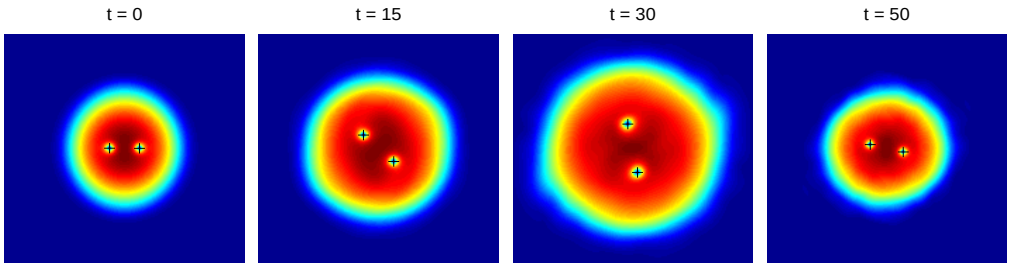

Figure 6: Plots of the density $|\psi(\mathbf{x},t)|$ for a vortex pair with $\mathbf{x}_{1,2}^0=(\pm 1,0)$ and $\beta=500$, where the displayed domain is $[-8,8]\times[-8,8]$.

located at $\mathbf{x}_2^0=(-x_0,0)$ with $x_0>0$, so that the initial distance between two vortex centers is $d_0=|\mathbf{x}_1^0-\mathbf{x}_2^0|=2x_0$.

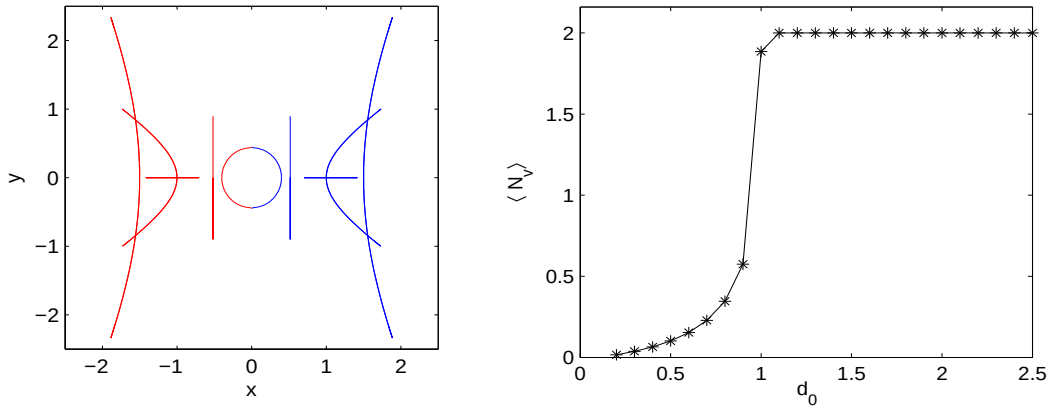

Figure 7: Trajectory of vortex dipoles for different x_0 (left) (from inside to outside $x_0=0.4$, $\sqrt{2-\sqrt{3}}$, $\sqrt{2}/2$, 1 and 1.5) and the average number of vortices $\langle N_v\rangle$ present in the time interval $[0,20]$ (right), where $\beta=0$.

We start our discussion by considering the case with $\beta=0$. Figure 7 displays the trajectory of the two vortex centers for different x_0, and it also shows the average number of vortices appearing in the condensate during the time $[0,20]$. From it, we find that when $\beta=0$, the dynamics of a vortex dipole is periodic with period $T=2\pi$, and there exists a critical initial distance $d_{0,c}=2\sqrt{2-\sqrt{3}}$. When $d_0\geq d_{0,c}$, the two vortices move 'parallel' and never collide with each other. Especially, when $d_0=d_{0,c}$, their trajectories are two straight lines parallel to the y-axis; when $d_0=\sqrt{2}$, they move along the x-axis. In addition, there are always two vortices in the condensate, i.e., $N_v(t)\equiv 2$, for $d_0\geq d_{0,c}$. On the other hand, when the initial distance $d_0<d_{0,c}$, the two vortices attract each other, and then they collide and disappear on the y-axis. The average number of vortices $\langle N_v\rangle$ implies that for some time after collision, there is no vortex existing in the condensate.

In addition, Figures 8-9 present a dynamics study of the phase and the position density for vortex dipoles with $x_0=0.4$ and $x_0=1$, respectively. When $x_0=0.4$, at $t=0$ the

two vortices attract each other and start moving 'down'. They meet on the y-axis within a short time, e.g. $t\approx 0.26$. Then for the time $t\in(0.26,2.88)$, no vortex exists in the condensate. At time $t\approx 2.88$, two vortices appear at the location where they annihilate, but their winding numbers are different from which they have before annihilating. For example, initially the vortex at the right half-plane has the winding number $m=+1$, while after reappearing it becomes $m=-1$. After it, the two vortices move back along the old trajectories and reach their initial positions at time $t=\pi$, and immediately the next half-period starts with the two vortices moving 'up'. Finally, at $t=2\pi$ the vortex dipole reaches their initial position with the initial winding numbers.

The dynamics of the vortex dipole with $x_0=1$ is quite different. When $t=0$, the two vortices start moving 'up' along two hyperbolas. At $t=\pi/2$, they have the largest distance, and at the same time they change their winding numbers to be opposite (i.e., from $+1$ to -1 or from -1 to $+1$). After it, the two vortices move back along the old trajectories and reach the original positions $(\pm x_0,0)$ at time $t=\pi$. The similar dynamics is repeated for $t\in[\pi,2\pi]$, but during this half period, they move along the hyperbolas which is below the x-axis.

Similarly, we have the following lemma for the dynamics of the vortex dipole when $\beta=0$ and $\Omega=0$:

Lemma 3.2. *When $\beta=0$ and $\Omega=0$ in (2.4), if the initial data $\psi_0(\mathbf{x})$ is chosen as (2.13) with $n=2$, $\mathbf{x}^0_{1,2}=(\pm x_0,0)$ and $m_{1,2}=\pm 1$, then the trajectory of the two vortex centers can be given by*

$$y(t)=\frac{2x_0^2-1}{x_0}\sin(t),\quad x_{1,2}(t)=\pm\sqrt{x_0^2[1+3\sin^2(t)]-y^2(t)},\qquad t\geq 0. \tag{3.10}$$

It is easy to see when $x_0\geq\sqrt{2-\sqrt{3}}$, the solutions in (3.10) are always real and $x_1(t)\neq x_2(t)$ for any $t\geq 0$, which indicates that the two vortices never meet. While when $x_0<\sqrt{2-\sqrt{3}}$, for some time t the solutions $x_1(t)$ and $x_2(t)$ become complex. By requiring that $x_1(t)=x_2(t)$, we obtain

$$|\sin(t)|=\sqrt{\left|\frac{x_0^4}{x_0^4-4x_0^2+1}\right|}, \tag{3.11}$$

that is, the solution t of (3.11) is the time when the two vortices meet each other. Furthermore, in every half-period $[k\pi,(k+1)\pi]$ (for $k=0,1,\ldots$) the first possible solution $t_{k,c}$ is the time when they collide and annihilate, while the second one $t_{k,r}$ represents the time when the two vortices reappear. For $t\in[t_{k,c},t_{k,r}]$, there is no vortex in the condensate.

In addition, we also study the case with asymmetric initial setup, and Figure 10 displays the trajectory of a vortex dipole with $\mathbf{x}_1^0=(0.9,0.1)$, $\mathbf{x}_2^0=(-1.1,0)$ and $m_1=-m_2=+1$. It shows that the slight change in the initial position may change the vortex trajectories considerably, but they are still confined to one half-plane of the condensate. This dynamics is still periodic with period $T=2\pi$.

When $\beta\neq 0$, the interaction of a vortex dipole becomes more complicated due to the effect of nonlinear term $\beta|\psi|^2\psi$ in (2.4). To get an insight about it, we first consider vortex

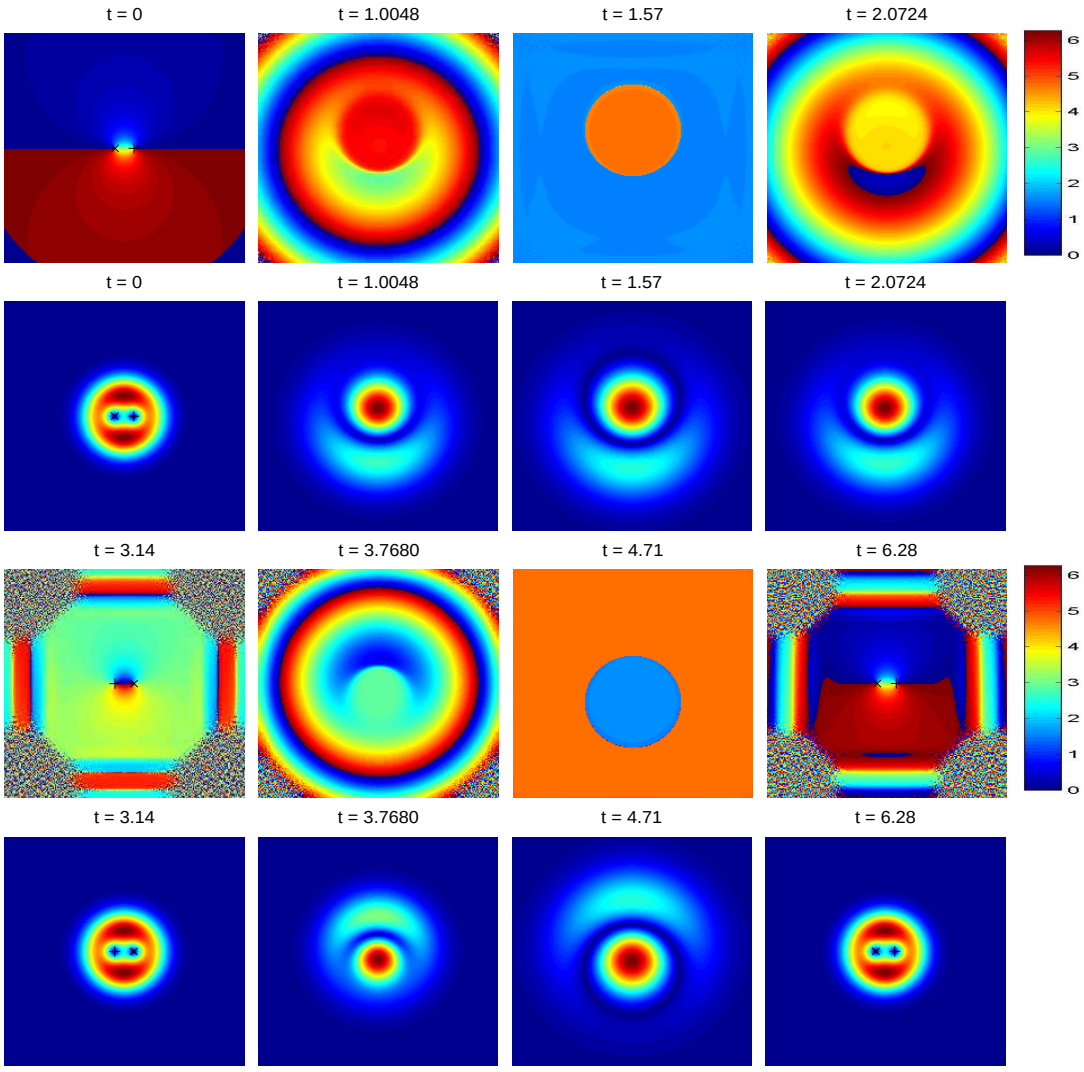

Figure 8: Plots of the phase $S(\mathbf{x},t)$ (above) and the density $|\psi(\mathbf{x},t)|$ (down) for a vortex dipole with $\mathbf{x}_{1,2}^0 = (\pm 0.4,0)$ and $\beta = 0$, where the displayed domain is $[-5,5]\times[-5,5]$.

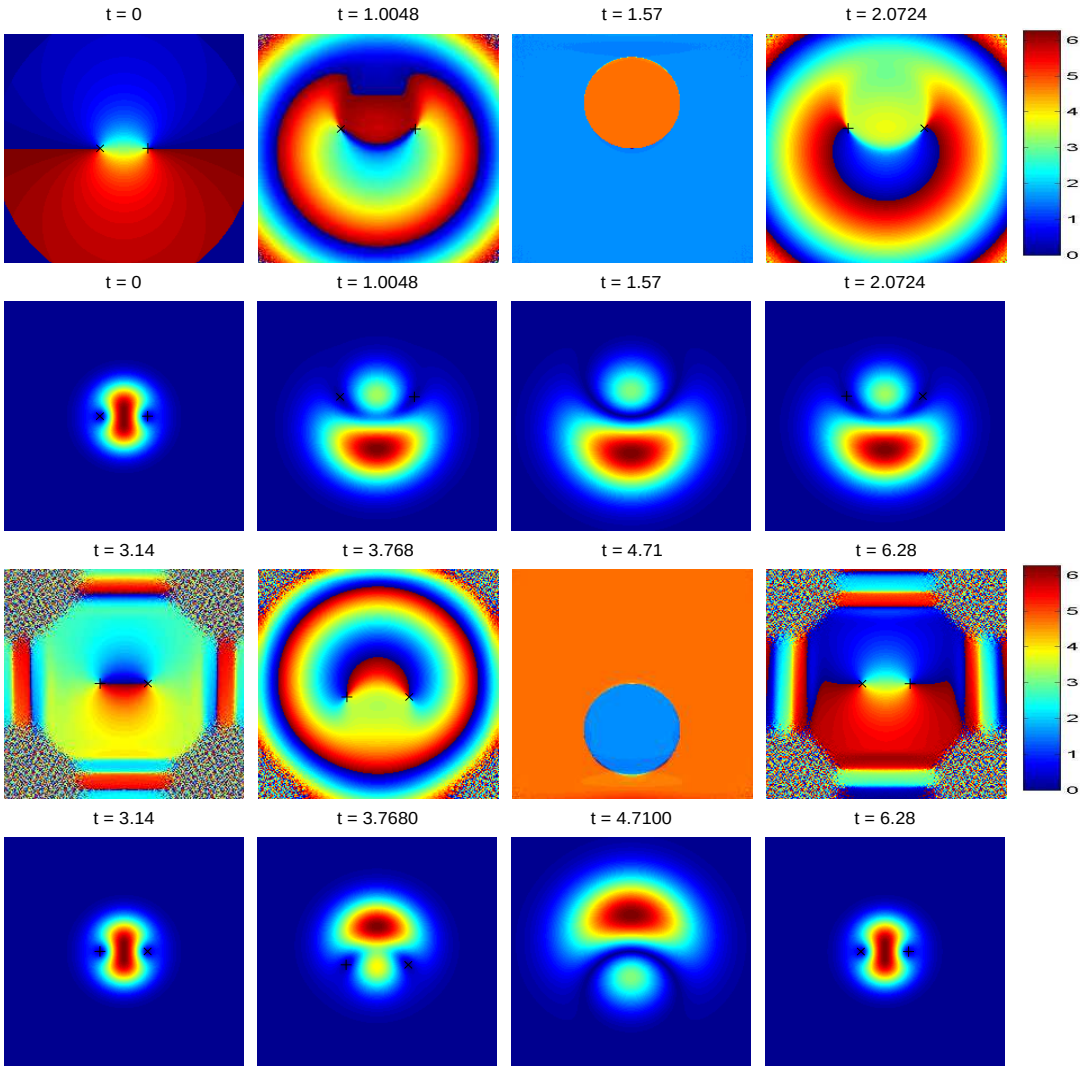

Figure 9: Plots of the phase $S(\mathbf{x},t)$ (above) and the density $|\psi(\mathbf{x},t)|$ (down) for a vortex dipole with $\mathbf{x}_{1,2}^0=(\pm 1,0)$ and $\beta=0$, where the displayed domain is $[-5,5]\times[-5,5]$.

dipoles in weakly interacting BECs with $\beta=1$. Figure 11 illustrates the trajectory of their centers for different initial distance d_0. In contrast to the situation when $\beta=0$, for any initial distance d_0 the two opposite vortices always collide and annihilate each other on the y-axis, and then a new vortex dipole is generated somewhere but different from their collision location. The dynamics is periodic with period $T\approx 2\pi$, and for different periods their trajectories are slightly changed.

Similarly, Figure 12 plots the trajectories of vortex dipoles in strongly interacting BECs for time $t\in[0,50]$, where the interaction parameter $\beta=500$. Furthermore, Figures 13-14

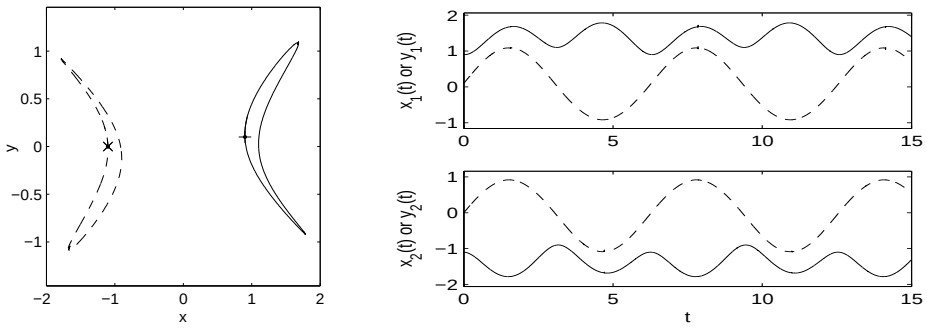

Figure 10: Trajectory (left) and time evolution (right) of $x_j(t)$ (solid line) and $y_j(t)$ (dashed line) for two vortex centers when the initial data is $\mathbf{x}_1^0=(0.9,0.1)$, $\mathbf{x}_2^0=(-1.1,0)$ and $m_1=-m_2=1$, where $\beta=0$.

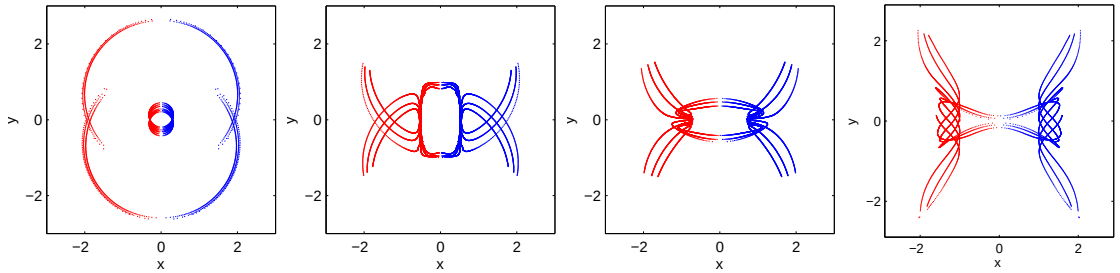

Figure 11: Trajectory of vortex dipoles in weakly interacting BECs with $\beta=1$, where from left to right: $d_0=0.6$, $2\sqrt{2-\sqrt{3}}$, $\sqrt{2}$ and 2.

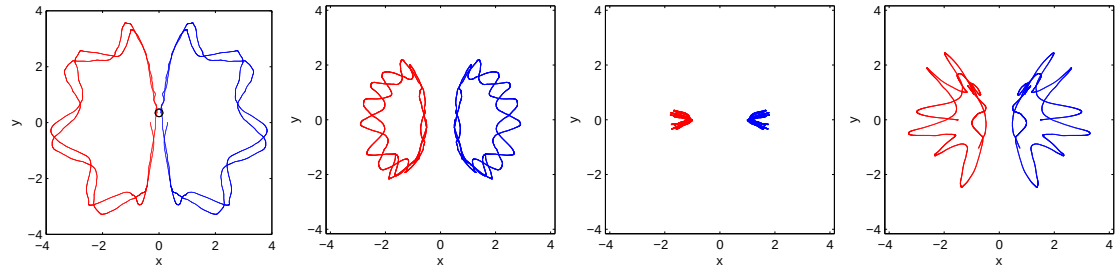

Figure 12: Trajectory of vortex dipoles in strongly interacting BECs with $\beta=500$, where from left to right: $d_0=0.6$, $2\sqrt{2-\sqrt{3}}$, 2 and 3, and the symbol 'o' represents the first collision position of two vortices.

show the dynamics of the position density $|\psi(\mathbf{x},t)|$ for $x_0=0.3$ and $x_0=1$, respectively. From them and our additional simulations, we find that if the initial distance d_0 is small, e.g. $d_0=0.6$, the two vortices meet each other in a short time and then they separate. After it, the two vortices still carry the same winding number as that they have before collision, which is quite different from the cases with small or zero β. On the other hand, if d_0 is large, they move in their own half-plane for a long time, and within our computational time, e.g. $t\in[0,200]$, they never meet each other. In addition, there are always two

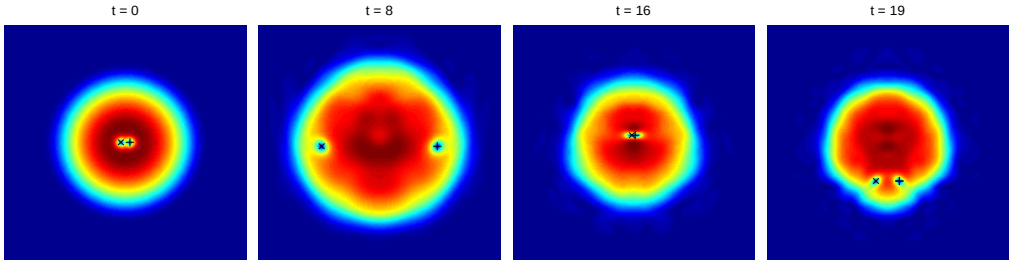

Figure 13: Plots of the density $|\psi(\mathbf{x},t)|$ for a vortex dipole with $\mathbf{x}_{1,2}^0=(\pm 0.3,0)$ and $\beta=500$, where the displayed domain is $[-8,8]\times[-8,8]$.

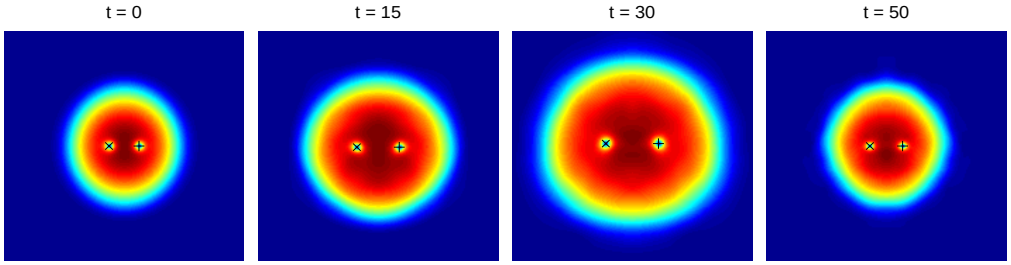

Figure 14: Plots of the density $|\psi(\mathbf{x},t)|$ for a vortex dipole with $\mathbf{x}_{1,2}^0=(\pm 1,0)$ and $\beta=500$, where the displayed domain is $[-8,8]\times[-8,8]$.

opposite vortices showing up in the condensate when $\beta\gg 1$.

3.3 Interaction of more vortices

In this section, we generalize our study on one or two vortices to $n\geq 3$ vortices which have the same or opposite winding numbers. For simplicity, we will focus only on the cases that at time $t=0$, the vortices are symmetrically located with respect to the potential center $(0,0)$. Typically, we consider the following three initial setups, and for each setup the interaction with $\beta=0$ and $\beta\gg 1$ (i.e. strongly interacting case) will be studied.

Case I: at $t=0$, the $n\geq 2$ vortices are uniformly located on a circle and they have the same winding number, i.e., for $j=1,2,\ldots,n$,

$$x_j^0=r_0\cos\left(\frac{2j\pi}{n}\right),\qquad y_j^0=r_0\sin\left(\frac{2j\pi}{n}\right),\qquad \text{with}\quad m_j=m, \tag{3.12}$$

with $r_0>0$ the radius of the circle and the winding number $m=+1$ or -1.

Case II: at $t=0$, the $n-1$ ($n\geq 3$) vortices are uniformly located on a circle, i.e.,

$$x_j^0=r_0\cos\left(\frac{2j\pi}{n-1}\right),\qquad y_j^0=r_0\sin\left(\frac{2j\pi}{n-1}\right),\qquad \text{with}\quad m_j=m \tag{3.13}$$

for $j=1,2,\ldots,n-1$, and the n-th vortex is located at the center,

$$x_n^0=y_n^0=0, \qquad \text{with} \quad m_n=m \tag{3.14}$$

with $r_0>0$ and $m=+1$ or -1.

Case III: the initial condition of the $n-1$ vortices satisfies (3.13) and

$$x_n^0=y_n^0=0, \qquad \text{with} \quad m_n=-m, \tag{3.15}$$

i.e., the vortex at the center of the circle has the opposite winding number.

When $\beta=0$, Figure 15 displays the trajectory of the vortices in Case I and Case II for different number n. For any time $t\geq 0$, the n vortices are always symmetric with respect to the trap center, and their dynamics is periodic with period $T=2\pi$. In Case I, if the number n is odd, then each vortex has a unique trajectory which is an ellipse. While if n is even, there are only $n/2$ different trajectories, and the j-th $(1\leq j\leq n/2)$ and $(j+n/2)$-th vortices share the same trajectory. In Case II, the motion of the first $n-1$ vortices is quite similar to that in Case I. Especially, the vortex initially located at $(0,0)$ never moves during the dynamics.

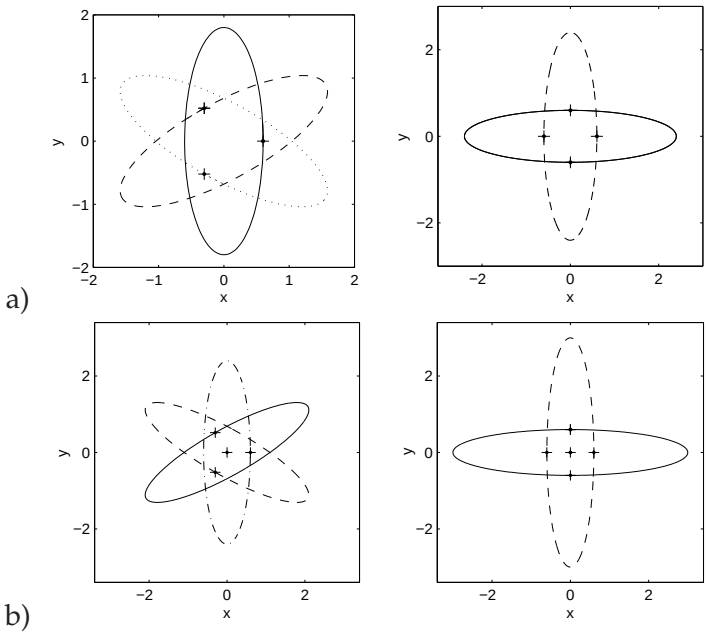

Figure 15: Trajectory of more vortices when $\beta=0$, $r_0=0.6$ and $m=+1$, where a) Case I with $n=3$ or 4; b) Case II with $n=4$ or 5.

Similar to the vortex pair and vortex dipole, we have the following lemma for the interaction of more vortices in Case I and Case II:

Lemma 3.3. *When $\beta=0$ and $\Omega=0$ in (2.4), if the initial data $\psi_0(\mathbf{x})$ is given by (2.13) with $\mathbf{x}_j^0$, for $j=1,2,\ldots,n$, satisfying (3.12) or (3.13)-(3.14), then the dynamics of the n vortex centers can be described by the following second-order ODE system:*

$$x_j''(t)+x_j(t)=0, \quad y_j''(t)+y_j(t)=0, \qquad t\geq 0, \quad j=1,2,\ldots,n, \tag{3.16}$$

with

$$x_j(0)=x_j^0, \quad y_j(0)=y_j^0, \quad x_j'(0)=-nmy_j^0, \quad y_j'(0)=nmx_j^0. \tag{3.17}$$

Especially, if we choose $n=2$ in Case I, then (3.16)-(3.17) collapses to the ODEs (3.6)-(3.7) in Lemma 3.1 with $\mathbf{x}_1^0=-\mathbf{x}_2^0$.

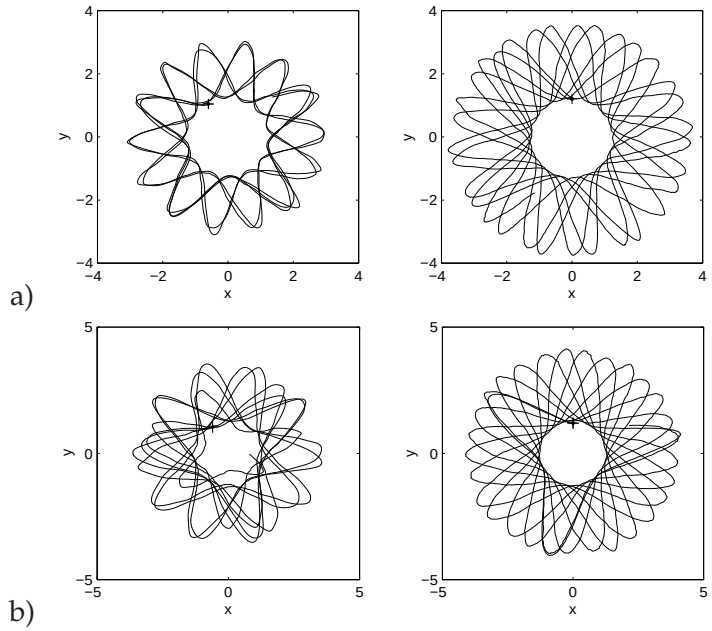

Figure 16: Trajectory of the 1-st vortex, i.e. $\mathbf{x}_1(t)$, for $t\in[0,100]$, when $\beta=200$, $r_0=1.2$ and $m=1$, where a) Case I with $n=3$ or 4; b) Case II with $n=4$ or 5.

Figure 16 presents the similar results for strongly interacting BECs, where $\beta=200$. Again it shows that the n vortices in Case I (or the first $n-1$ vortices in Case II) are always symmetric with respect to $(0,0)$, and especially in Case II, $\mathbf{x}_n(t)\equiv(0,0)$ for any time $t\geq 0$. When $\beta\neq 0$, each vortex has its unique trajectory, which is different from the case with $\beta=0$.

If the n vortices carry different winding numbers, their interaction highly depends on the initial distance. For simplicity, Figure 17 shows the trajectory of the vortex centers only for a large $r_0=0.85$ and $\beta=0$. In addition, Figure 18 plots the time evolution of the position density $|\psi(\mathbf{x},t)|$ for the case with $n=5$.

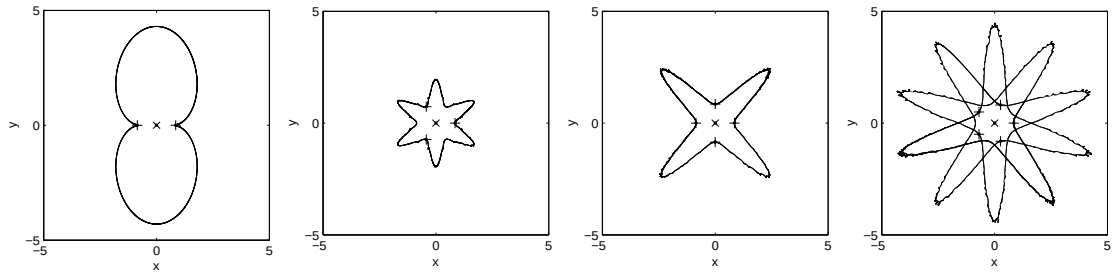

Figure 17: Trajectory of more vortices in Case III with a large $r_0 = 0.85$, $m = 1$ and $\beta = 0$, where from left to right: $n = 3$, 4, 5 and 6.

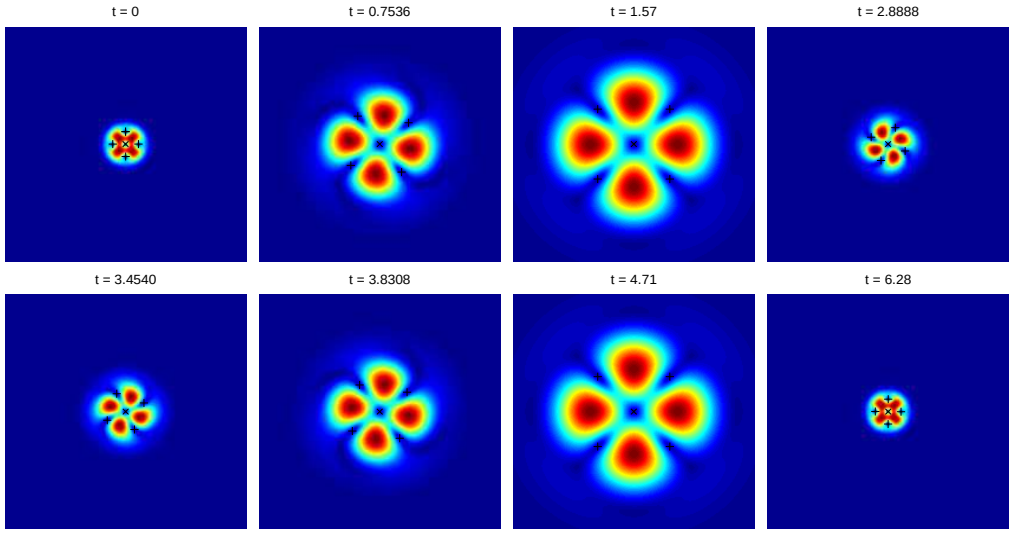

Figure 18: Plots of and the density $|\psi(\mathbf{x},t)|$ for 5 vortices in Case III, where $r_0 = 0.85$, $\beta = 0$, and the displayed domain is $[-8,8]\times[-8,8]$.

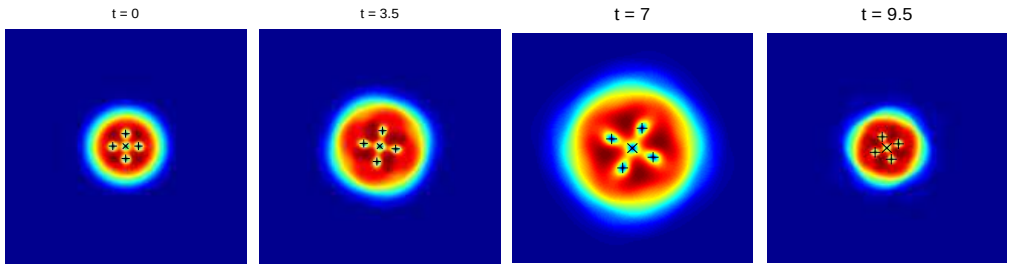

Figure 19: Plots of the density $|\psi(\mathbf{x},t)|$ for 5 vortices in Case III, where $r_0 = 0.85$, $\beta = 200$, and the displayed domain is $[-8,8]\times[-8,8]$.

From it and our additional computations, we find that the vortex initially located at the center never moves for any time $t \geq 0$. If r_0 is small, the other $n-1$ vortices are

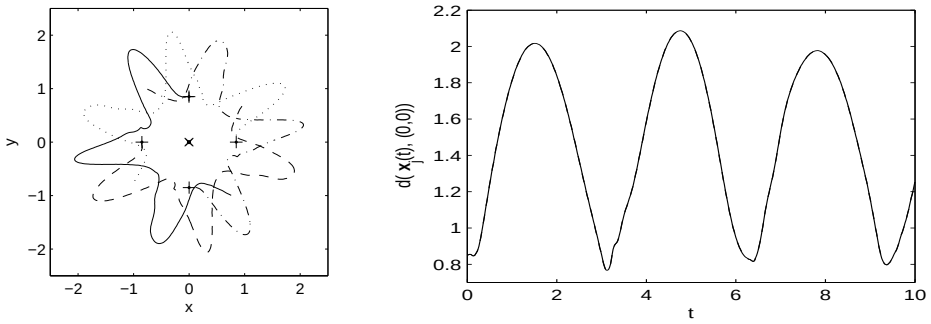

Figure 20: Trajectory of the vortex centers (left) and their distance to the trap center (right) in Case III, where $n=4$, $r_0=0.85$, and $\beta=200$.

attracted to the center and collide there; after some time, new vortices are generated in the condensate. This dynamics is repeated periodically. While if r_0 is large, they move periodically but never collide with each other, and the $n-1$ vortices initially on a circle share exactly the same trajectory. In addition, to compared with the dynamics when $\beta=0$, Figures 19-20 show the time evolution of the density $|\psi(\mathbf{x},t)|$ and the trajectory of the vortex centers for the case with $\beta=200$. When β is large, there are always 5 vortices in the condensate. The first 4 vortices are always on a circle with its center at $(0,0)$. Different from the case with $\beta=0$, each vortex has a unique trajectory, and the dynamics is not periodic.

4 Vortices in rotating BECs

As we have seen, in nonrotating condensates, the dynamics and interaction of vortices highly depends on the nonlinearity parameter β. If the vortices have opposite winding numbers, it also depends on the initial distance between vortex centers. In rotating BECs, i.e., an angular rotation is imposed on the condensate, the situation becomes much more complicated and interesting. We find the following lemma to describe the relation of the vortex interaction in nonrotating and rotating BECs:

Lemma 4.1. *Choose the initial data $\psi_0(\mathbf{x})$ as (2.13). For any fixed $\beta\geq 0$, assume that $(x_j(t),y_j(t))$ describes the trajectory of the j-th vortex in nonrotating BECs, and respectively, $(\widetilde{x}_{j,\Omega}(t),\widetilde{y}_{j,\Omega}(t))$ is that in rotating BECs with the rotation speed Ω and the same nonlinearity β. Then we have*

$$\widetilde{x}_{j,\Omega}(t)=x_j(t)\cos(\Omega t)+y_j(t)\sin(\Omega t), \tag{4.1}$$
$$\widetilde{y}_{j,\Omega}(t)=y_j(t)\cos(\Omega t)-x_j(t)\sin(\Omega t), \qquad t\geq 0, \quad j=1,2,\ldots,n. \tag{4.2}$$

It is easy to get

$$\big[\widetilde{x}_{j,\Omega}(t)\big]^2+\big[\widetilde{y}_{j,\Omega}(t)\big]^2=\big[x_j(t)\big]^2+\big[y_j(t)\big]^2, \qquad t\geq 0. \tag{4.3}$$

That is, at time $t \geq 0$, the distance between the j-th vortex and the trap center is independent of the rotational speed Ω.

Thus if we know the dynamics of the vortices in nonrotating BECs, we can easily generalize it to rotating BECs by applying (4.1)-(4.2). To verify the conclusions in Lemma 4.1, we numerically study the dynamics and interaction of vortices by solving the GPE (2.4)-(2.5) in a rotating frame.

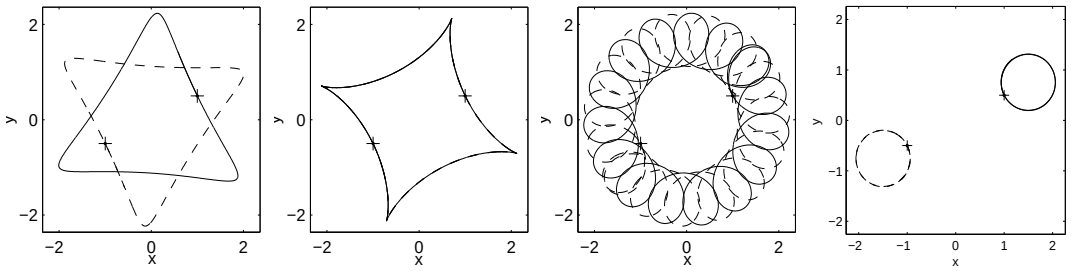

Figure 21: Trajectory of vortex pairs in rotating BECs with $\beta = 0$ and $\mathbf{x}_{1,2}^0 = (\pm 1, \pm 0.5)$. From left to right: $\Omega = 1/3, 1/2, \sqrt{3}/2$, and 1.

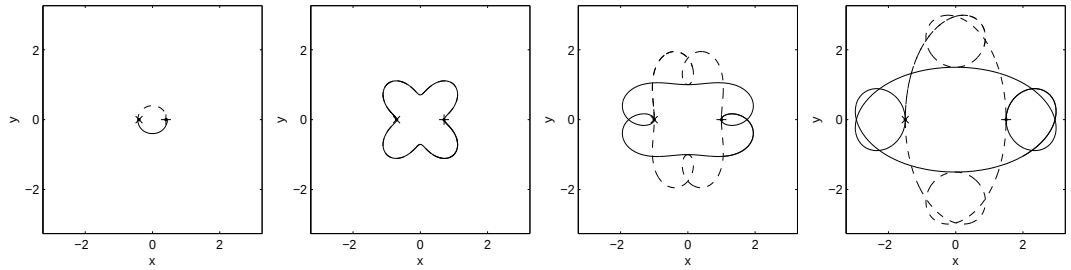

Figure 22: Trajectory of vortex dipoles in rotating BECs with $\beta = 0$ and $\Omega = 0.5$. From left to right: $d_0 = 0.8, \sqrt{2}, 2$, and 3.

To compare with the analytical results in (4.1)-(4.2), Figures 21-22 illustrate the numerical results for a vortex pair and a vortex dipole, respectively. In addition, Figure 23 presents the phase and density plots for a vortex dipole with $\mathbf{x}_{1,2}^0 = (\pm 1, 0)$, $\beta = 0$ and $\Omega = 0.5$. From Fig. 21 and our additional results not shown here, we find that the vortices having the same winding numbers never collide, and if their initial position are symmetric with respect to the potential center, then they preserve the symmetry for any time $t \geq 0$. As we have known, if $\beta = 0$, the dynamics in nonrotating BECs is periodic with period $T = 2\pi$. However, for rotating BECs the periodicity also depends on Ω. For example, when $\beta = 0$, if Ω is a rational number, i.e., $|\Omega| = q/p$ with q and p positive integers and no common factor, the two vortices rotate periodically. Furthermore, if both p and q are odd integers, the period $T = p\pi$, and the trajectories of two vortex centers are different; otherwise $T = 2p\pi$, and they have exactly the same trajectories. While if Ω is irrational, the vortices would move within a bounded region. Similar to the nonrotating case, the

interaction of a vortex dipole highly depends on their initial distance, and the critical distance for $\beta=0$ is still $d_{0,c}=2\sqrt{2-\sqrt{3}}$. The phase and density plots in Fig. 23 show that when $\Omega=1/2$ $(q=1,p=2)$, the period is $T=2p\pi=4\pi$, which confirms our analytical results in Lemma 4.1.

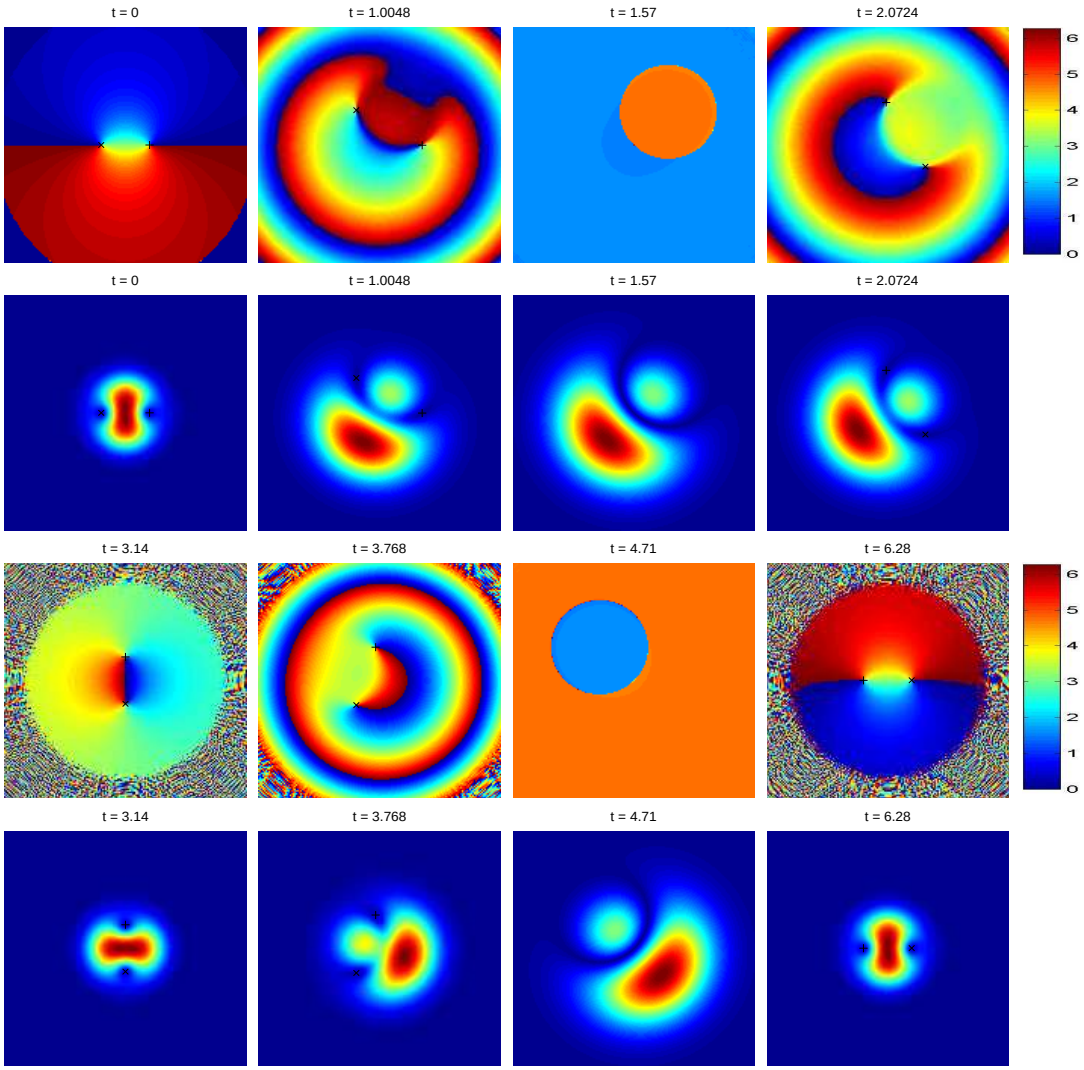

Figure 23: Plots of the phase $S(\mathbf{x},t)$ (above) and the density $|\psi(\mathbf{x},t)|$ (down) for a vortex dipole with $\mathbf{x}_{1,2}^0=(\pm1,0)$, $\beta=0$ and $\Omega=0.5$, where the displayed domain is $[-5,5]\times[-5,5]$.

5 Summary and conclusion

We have studied the dynamics and interaction of vortices in Bose-Einstein condensates (BECs) based on the two-dimensional Gross-Pitaevskii equation (GPE) with/without an angular momentum rotation term.

In nonrotating BECs, the interactions of two vortices were investigated in detail for different interatomic interaction β. If the two vortices have the same winding number, they would rotate (clockwise if $m=-1$ or counter clockwise if $m=+1$) around the trap center for any $t \geq 0$ but never meet each other. In contrast, the interaction of a vortex dipole highly depends on the initial distance between their centers. When $\beta=0$, we found that the dynamics of both the vortex pair and vortex dipole are periodic with period $T=2\pi$. Furthermore, some analytical results were derived to describe the motion of the vortex centers. The situation becomes considerably different if $\beta \neq 0$, and we numerically studied the interaction in both weakly and strongly interacting condensates. When $\beta \gg 1$, there are always two vortices in the condensate. Some important findings were obtained to provide the further understanding of vortex interactions in BECs. We also generalized the study of two vortices to more vortices with some symmetric initial setup.

The interaction of vortices in rotating BECs becomes more interesting, and it depends not only on the winding number m and the parameter β, but on the rotation speed Ω. We found the analytical expressions to describe the relation between the interaction in nonrotating and rotating BECs. Some numerical results were also provided to verify the analytical findings.

Acknowledgments

The author acknowledges the supports from the US Department of Energy under grant number DE-FG02-05ER25698, and thanks valuable discussions with Professor Weizhu Bao on the subject. This work was partially done while the author was visiting the Institute for Mathematical Science, National University of Singapore, in 2007.

References

[1] M. R. Matthews, B. P. Anderson, P. C. Haljan, D. S. Hall, C. E. Wieman and E. A. Cornell, Phys. Rev. Lett. 83, 2498 (1999).
[2] K. W. Madison, F. Chevy, W. Wohlleben and J. Dalibard, Phys. Rev. Lett. 84, 806 (2000).
[3] K. W. Madison, F. Chevy, W. Wohlleben and J. Dalibard, J. Mod. Opt. 47, 2715 (2000).
[4] A. E. Leanhardt, A. Görlitz, A. P. Chikkatur, D. Kielpinski, Y. Shin, D. E. Pritchard and W. Ketterle, Phys. Rev. Lett. 89, 190403 (2002).
[5] Y. Castin, Z. Hadzibabic, S. Stock, J. Dalibard and S. Stringari, Phys. Rev. Lett. 96, 040405 (2006).
[6] K. T. Kapale and J. P. Dowling, Phys. Rev. Lett. 95, 173601 (2005).
[7] V. M. Pérez-García and M. A. García-March, Phys. Rev. A 75, 033618 (2007).

[8] L.-C. Crasovan, G. Molina-Terriza, J. P. Torres, L. Torner, V. M. Pérez-García and D. Mihalache, Phys. Rev. E 66, 036612 (2002).
[9] L. -C. Crasovan, V. Vekslerchik, V. M. Pérez-García, J. P. Torres, D. Mihalache and L. Torner, Phys. Rev. A 68, 063609 (2003).
[10] M. Möttönen, S. M. M. Virtanen, T. Isoshima and M. M. Salomaa, Phys. Rev. A 71, 033626 (2005).
[11] V. Pietilä, M. Möttönen, T. Isoshima, J. A. M. Huhtamäki and S. M. M. Virtanen, Phys. Rev. A 74, 023603 (2006).
[12] A. Klein, D. Jaksch, Y. Zhang and W. Bao, Phys. Rev. A 76, 043602 (2007).
[13] J. -P. Martikainen, K. -A. Suominen, L. Santos, T. Schulte and A. Sanpera, Phys. Rev. A 64, 063602 (2001).
[14] Q. Zhou and H. Zhai, Phys. Rev. A 70, 043619 (2004).
[15] Y. Castin and R. Dum, Eur. Phys. J. D. 7, 399 (1999).
[16] D. L. Feder, C. W. Clark and B. I. Schneider, Phys. Rev. A 61, 011601 (1999).
[17] W. Bao and Y. Zhang, Math. Mod. Meth. Appl. Sci. 15, 1863 (2005).
[18] W. Bao, Q. Du and Y. Zhang, SIAM J. Appl. Math. 66, 758 (2006).
[19] Y. Zhang, W. Bao and Q. Du, SIAM J. Appl. Math. 67, 1740 (2007).
[20] Y. Zhang, W. Bao and Q. Du, Eur. J. Appl. Math. 18, 607 (2007).
[21] W. Bao, R. Zeng and Y. Zhang, Physica D 237, 2391 (2008).
[22] L. S. Peranich, J. Comput. Phys. 68, 501 (1987).
[23] F.-Y. Zhang and S.-J. Lu, J. Comput. Math. 19, 393 (2001).
[24] R. Ciegis and V. Pakalnyte, Internat. J. Appl. Sci. Comput. 8, 127 (2001).
[25] A. Minguzzi, S. Succi, F. Toschi, M. P. Tosi and P. Vignolo, Phys. Rep. 395, 223 (2004).
[26] S. Palpacelli and S. Succi, Commun. Comput. Phys. 4, 980 (2008).
[27] Y. Zhang and W. Bao, Appl. Numer. Math. 57, 697 (2007).
[28] J. J. García-Ripoll, V. M. Pérez-García and V. Vekslerchik, Phys. Rev. E 64, 056602 (2001).
[29] I. Bialynicki-Birula and Z. Bialynicka-Birula, Phys. Rev. A 65, 063606 (2002).